EFFECTS OF GAS RELATIVE PERMEABILITY HYSTERESIS AND SOLUBILITY ON ASSOCIATED CO_2 STORAGE PERFORMANCE

Lu Jin,* Lawrence J. Pekot, Steven A. Smith, Olarinre Salako, Kyle J. Peterson, Nicholas W. Bosshart, John A. Hamling, Blaise A.F. Mibeck, John P. Hurley, Christopher J. Beddoe, and Charles D. Gorecki

*Corresponding Author: E-Mail: ljin@undeerc.org
Phone: 1-701-777-5316; Fax: 1-701-777-5181
E-Mail: lpekot@undeerc.org
E-Mail: ssmith@undeerc.org
E-Mail: osalako@undeerc.org
E-Mail: kpeterson@undeerc.org
E-Mail: nbosshart@undeerc.org
E-Mail: jhamling@undeerc.org
E-Mail: bmibeck@undeerc.org
E-Mail: jhurley@undeerc.org
E-Mail: cbeddoe@undeerc.org
E-Mail: cgorecki@undeerc.org

University of North Dakota, Energy & Environmental Research Center, 15 North 23rd Street, Stop 9018, Grand Forks, ND 58202-9018

ABSTRACT

CO_2 enhanced oil recovery (EOR) has been carried out in the Bell Creek oil field since 2013. Together with the encouraging oil production results, a considerable quantity of CO_2 has also been trapped in the reservoir as a normal part of the EOR process, also referred to as associated storage. Because of the complex geologic conditions in the field, a series of experimental and modeling work have been conducted to better understand the CO_2 EOR and associated storage performance in the reservoir. Effects of gas relative permeability hysteresis and solubility on associated CO_2 storage performance are thoroughly investigated in this study.

A proportion of injected CO_2 remains behind through residual and solubility trapping mechanisms when CO_2 flows through a reservoir during a CO_2 EOR process. Over 50 core plugs were collected from the reservoir to characterize the rock properties. Mineralogical analysis and capillary pressure measurements showed that the mineral composition and pore-size distribution in the reservoir are favorable for residual trapping of CO_2. The hysteresis of gas relative permeability was measured to assess the effect of residual trapping on associated CO_2 storage using steady-state relative permeability tests and reservoir simulation. The reservoir oil was characterized based on pressure–volume–temperature experiments and Peng–Robinson equation of state modeling, which showed that CO_2 solubility in oil is much greater ($\geq$ 5 times) than in water. Results indicated that depleted oil reservoirs have great potential to store a huge quantity of CO_2 associated with EOR operations, as residual oil saturation is 0.3 or greater in most conventional oil reservoirs after water flooding.

KEYWORDS: CO_2 enhanced oil recovery, associated CO_2 storage, relative permeability hysteresis, residual trapping, solubility trapping

1. INTRODUCTION

CO_2 trapping and associated storage processes are important to enhanced oil recovery (EOR) performance, as they can affect the oil recovery and CO_2 utilization factor (Belhaj et al., 2013; Gozalpour et al., 2005; Kovscek, 2002; Malik and Islam, 2000; Verma, 2015; Soltanian et al. 2017). For instance, more trapped CO_2 may lead to a higher CO_2 utilization factor since less CO_2 is available to contact oil and sweep it from the reservoir; therefore, more CO_2 needs to be purchased and injected for an equivalent oil recovery (Gao et al., 2013; Jin et al., 2017b; Li et al., 2006; Zhang et al., 2010). The trapping mechanisms also determine the state of the associated CO_2 storage during and after CO_2 flooding. Fig. 1 is a generalized illustration which shows how the contribution from different trapping mechanisms change over time leading to an increase in CO_2 trapping strength (or security) (Metz et al., 2005). Effective trapping mechanisms ensure injected CO_2 will remain, in permanence, within the area of review (limited lateral migration) and contained within the zone of interest (limited vertical migration). The four primary CO_2-trapping mechanisms include structural/stratigraphic, residual, solubility, and mineral trapping in most conventional petroleum reservoirs (Jia et al., 2016). Adsorption trapping is an important mechanism in unconventional reservoirs, such as shale oil, shale gas, and coalbed methane (CBM) reservoirs, as these reservoirs have higher percentages (>5%) of organic content and a large number of nanometer-size pores (Wong et al., 2007; Busch et al., 2008; Gale and Freund, 2001; Jia et al., 2017; Jin et al., 2016, 2017a; Khosrokhavar et al., 2014; Ross and Bustin, 2009). Mineral trapping, with the exception of a small number of documented instances of CO_2 storage in basalt formations (McGrail et al., 2016, 2006), is thought to occur over an extended time frame (hundreds to thousands of years).

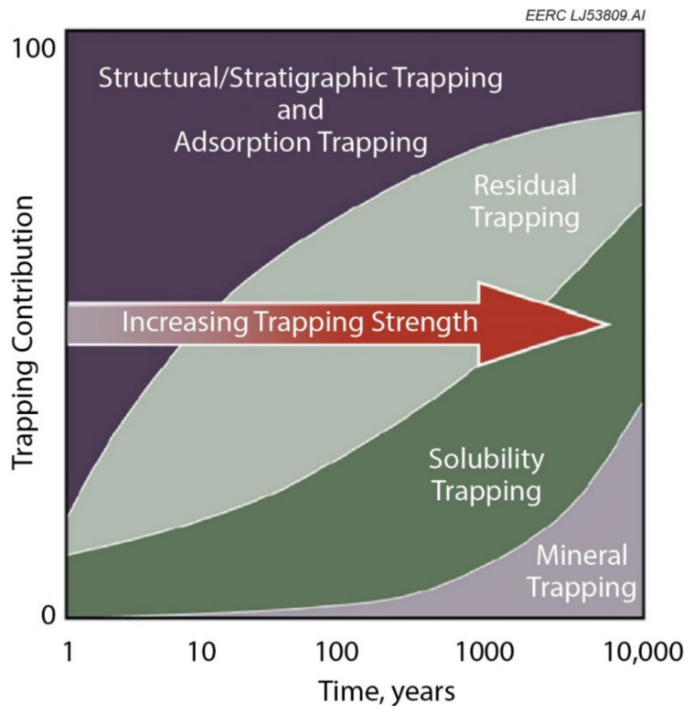

Fig. 1. Increase of CO_2 trapping strength with time (modified from Intergovernmental Panel on Climate Change, 2005).

Studies have shown that residual CO_2 saturation may be on the order of 5%–30%, varying with reservoir conditions (Ennis-King and Paterson, 2001; Juanes et al., 2006; Niu et al., 2015; Zuo and Benson, 2014). Therefore, understanding residual trapping in a reservoir can provide a conservative estimate of CO_2 storage potential for sequestration projects (Burnside and Naylor, 2014; Krevor et al., 2015; Al-Menhali and Krevor, 2016). The residual trapping of CO_2 in a small pore space has been visualized and analyzed accurately at core scale (Iglauer et al., 2011; Ruprecht et al., 2014). Using core-flooding with x-ray computed tomography, the results indicated that the hysteretic nonwetting phase behavior (i.e., relative permeability hysteresis of CO_2) would be a significant factor in determining long-term immobilization of injected CO_2 in the reservoir. Accurate determination of relative permeability hysteresis is also important for CO_2-based EOR projects since many of them use water alternating gas (WAG) operations, where CO_2 hysteresis directly relates to the displacing efficiency (Fatemi et al., 2012).

CO_2 dissolves in other formation fluids when injected into a reservoir, a process termed solubility trapping. The density of oil increases when CO_2 is dissolved in the oil (Holm and Josendal, 1974), which may create gravitational instability in the reservoir, leading to convective mixing of fluids. The mixing of fluids with differing dissolved CO_2 content will further enhance the dissolution process in the long run (Li and Jiang, 2014; Shelton et al., 2016; Szulczewski et al., 2013). Therefore, CO_2 dissolution is considered a significant trapping mechanism in deep geologic formations, with potential to permanently store large amounts of CO_2 (Ampomah et al., 2016; Bachu and Adams, 2003; Bachu and Bennion, 2007; Metz et al., 2005; Holubnyak et al., 2018).

A literature review showed that most of the studies on CO_2-trapping mechanisms are based on dedicated CO_2 storage in deep saline formations (Al-Khdheeawi et al., 2018; Bachu and Adams, 2003; Bachu and Bennion, 2007; Burnside and Naylor, 2014; Iglauer, 2011; Juanes et al., 2006; Krevor et al., 2015; Szulczewski et al., 2013). The effects of these mechanisms on associated CO_2 storage during EOR operations have not been discussed thoroughly. There is still a lack of rock and fluid characterization data from actual oil fields to clearly demonstrate the correlations between these trapping mechanisms and associated CO_2 storage performance. In this study, a series of experimental and simulation work has been conducted to investigate the effects of residual and solubility trapping mechanisms on associated CO_2 storage performance in the Bell Creek oil field, where CO_2-based EOR operations are in progress. This is part of a larger study on CO_2 associated storage being conducted by the Plains CO_2 Reduction (PCOR) Partnership at the Bell Creek oil field in southeastern Montana (Braunberger et al., 2014; Gorecki et al., 2013; Hamling et al., 2013; 2016).

2. CO_2 EOR AND ASSOCIATED STORAGE IN THE BELL CREEK OIL FIELD

Since discovery in 1967, the Bell Creek oil field has undergone primary production (solution gas drive), waterflooding, and two micellar–polymer pilot tests and CO_2-based EOR since 2013. Over 40 years of waterflooding in the field has resulted in a reservoir saturated with water and with oil at residual saturation levels ~30%–45%. Fig. 2 shows the encouraging oil production performance of the field from the beginning of CO_2 injection. The oil production rate has increased from 7 thousand barrels per month (bpm) to 110 thousand bpm, which has yielded over 2.4 MMbbl of oil in the first 3 years of EOR operations. CO_2 injection increased from 9.5 to 234.5 thousand tonnes per month (tpm) in the first 2 years of injection and then fluctuated around 195 thousand tpm after June 2015, as shown in Fig. 3 (Montana Board of Oil and Gas Conservation, 2017). CO_2 production lagged behind the injection for about 9 months, indicating that CO_2 can effectively displace oil in the pore space and remain in place during flooding operations. About 5 million tonnes of CO_2 has been injected into the reservoir, and over 3 million tonnes has been stored there since the beginning of CO_2 flooding (as of March 2016). From Fig. 3, it is also clear that the gas storage rate related closely to the injection rate, decreasing rapidly when the injection became stable, after June 2015, while the production rate continued increasing. This observation indicates that CO_2 dominated the flow networks between injection and production wells and likely means gas production will continue to increase as the flooding goes on.

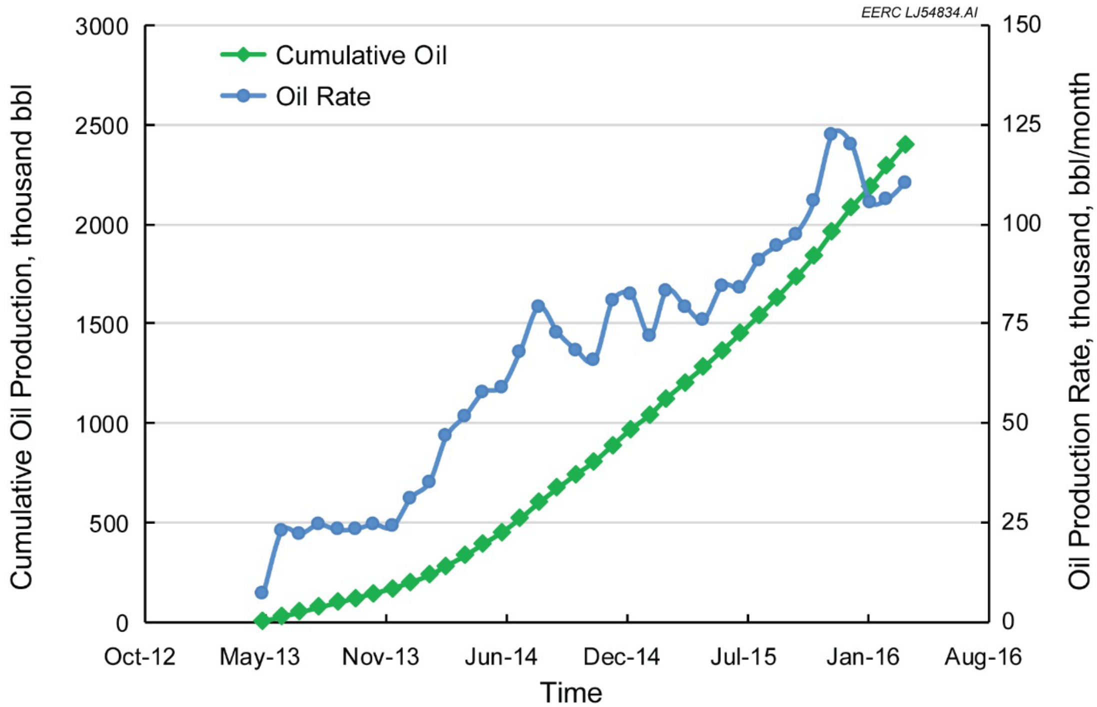

Fig. 2. Oil production performance during the Bell Creek CO_2-flooding process.

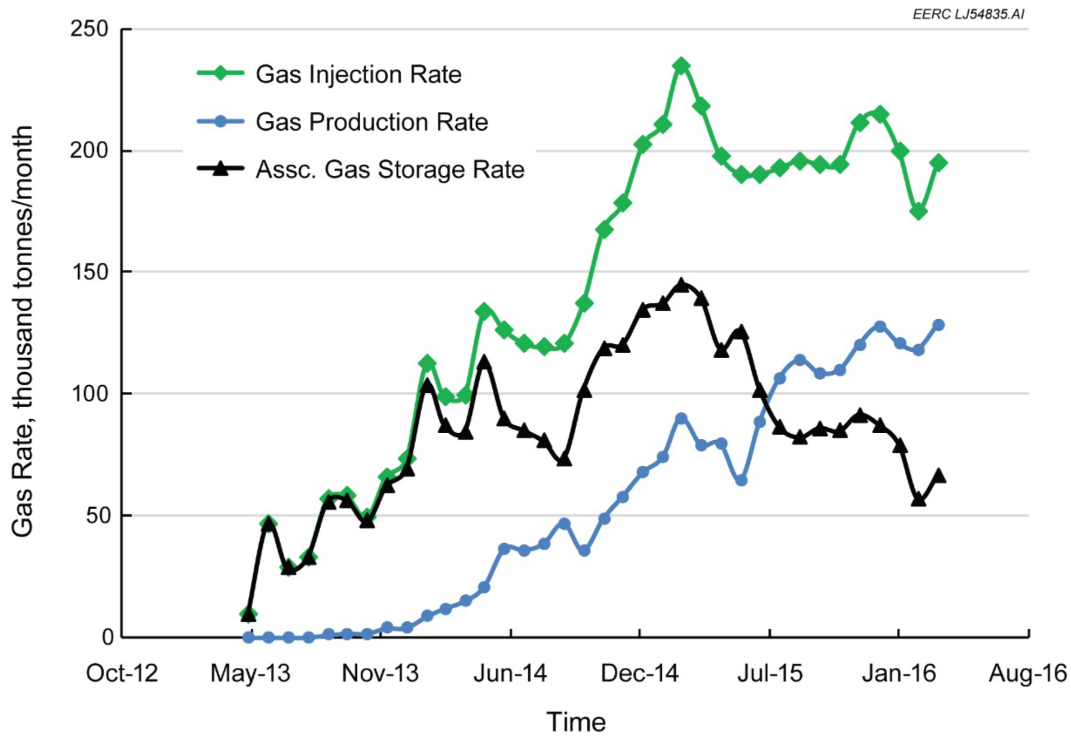

Fig. 3. Gas production, injection, and storage rates in the Bell Creek oil field.

Of the primary CO_2-trapping mechanisms shown in Fig. 1, the mineral trapping is of decreased importance when immediate containment/conformity of injected CO_2 is considered, and the effect of adsorption trapping is minimal since there is a lack of organic content in this conventional reservoir. Therefore, these two mechanisms will likely have no impacts on operational activities in the Bell Creek oil field. As such, CO_2 mineralization and adsorption have not been a focus and will not be discussed further. Since the reservoir is strongly heterogeneous and the CO_2 floods operations are conducted using WAG, the residual and solubility trapping mechanisms are important for the CO_2 flow behavior in the Bell Creek oil field and, therefore, were investigated and are discussed in the following sections.

3. RESIDUAL TRAPPING OF CO_2

Residual trapping occurs rapidly after CO_2 is injected into the formation under the effects of wettability and capillary pressure, resulting in immobilization of CO_2 in the pore space (Afonja et al., 2012; Al-Khdheeawi et al., 2018; Krevor et al., 2012, 2015; Raza et al., 2015, 2016). Relative permeability is a concept used to describe individual fluid-phase mobility when multiple fluid phases are present while accounting for wettability and capillary pressure phenomena. Injection of CO_2 results in increasing near-wellbore CO_2 saturation (which continues to increase away from the injection point as injection progresses) accompanied by a decrease in brine/oil saturation, in which case relative permeability of CO_2 increases. After injection ends as CO_2 migrates updip, or if water is injected after CO_2, the near wellbore CO_2 saturation will decrease away from the injection point with (accompanied by an increase in brine/oil saturation), so the relative permeability of CO_2 decreases. As CO_2 saturation decreases, a “residual” saturation will eventually be reached at which CO_2 is effectively immobilized and, therefore, considered stabilized under the effects of residual CO_2 trapping (Spiteri et al., 2008). Thus predicting the extent of CO_2 migration within the reservoir under the effects of residual trapping requires an estimate of residual CO_2 saturation.

An additional complexity is that the shape of relative permeability curves may be different depending on the directionality of changing fluid saturations (imbibition versus drainage), termed relative permeability hysteresis. The replacement of in situ liquid by injected CO_2 is termed drainage (nonwetting gas phase replaces the wetting liquid phase). In the WAG injection process, the gas and liquid phases alternately displace each other, meaning the drainage and imbibition processes occur in cycles. Hysteresis occurs under the effects of wettability and capillary pressure when CO_2 is present. This is important to understand in investigations of CO_2 storage, as the effect is usually pronounced when multiple fluids occupy the same system and may have direct implications to CO_2 migration and the trapping of CO_2 in the pore space (Burnside and Naylor, 2014). Rock properties, such as mineral composition and pore-size distribution (PSD), play fundamental roles in understanding the capillary effects and residual trapping in the reservoir.

Over 50 core plugs were collected from different wells which penetrate through the main sandstone of the reservoir. A detailed evaluation of rock properties was conducted using photomicrography and x-ray diffraction (XRD) mineralogical analysis to visualize the rock framework and determine the mineral composition of the rock. The Bruker D8 x-ray diffractometer was used to make the XRD measurements. The model can examine samples in situ using noncorrosive gas environments from vacuum to 147 psi and up to 900°C in temperature. Ten rock samples (including seven sandstone cores from the pay zone and three shale cores from the cap rock) were characterized using XRD to ensure that the results are representative of the reservoir. Generally, the results of sandstone cores are very similar. Figs. 4a and 4b show the typical photomicrograph and mineral composition of a rock sample from the main sandstone in the reservoir, respectively. The figure shows that quartz is the main mineral component (78 wt%) in the oil-bearing sand. The quartz grains are poorly to moderately sorted, and most of them are angular to subangular, with relatively sharp edges. The framework elements also include pebble-size petrified wood fragments, and the matrix is mainly mudstone which constitutes about 13 wt% of the rock. The clay mineralogy mainly includes smectite, illite, and mica, which makes the rock more favorable for residual trapping of CO_2 because of the high capillary pressure caused by the small pore throat sizes between the clay particles.

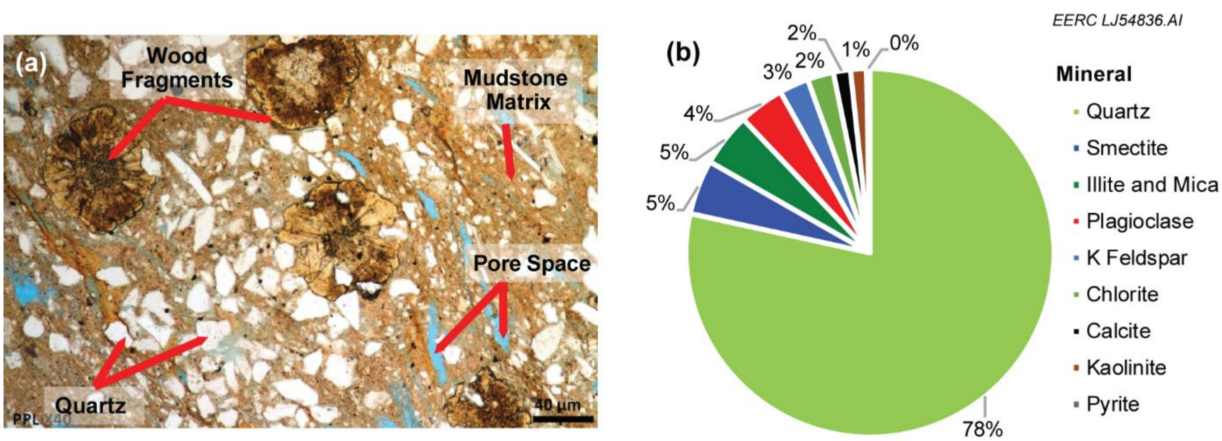

Fig. 4. Photomicrograph (a) and mineral composition (b) of a rock sample from the main sandstone in the reservoir.

Eq. 1 shows the relation between capillary pressure and pore throat size (Ahmed, 2006):

$$P_c = \frac{2\sigma cos\theta}{r} \quad \text{[Eq. 1]}$$

Where P_c is the capillary pressure, *kPa*; σ is the interfacial tension (IFT), *dyne/cm*; Θ is the contact angle between two phases, *degree*; and r is the pore throat radius, μm.

The equation shows that tiny pore throats can generate a considerable capillary pressure between phases when two or more fluids, i.e., CO_2, oil, and/or water, coexist in the rock. Capillary pressure curves were measured using a high-pressure mercury injection (HPMI) method for the selected samples. A typical curve is shown in Fig. 5, which indicates that the capillary effect could be quite strong when the nonwetting phase enters the small pores.

PSD can be determined based on the rock–fluid properties and capillary pressure curve, as shown in Fig. 6. The figure indicates that most of the pores in the rock belong to macro- and megapores, which have a throat radius greater than 5 µm. However, 20% of the pores have a throat radii of less than 2.5 µm. These small pores may have effects on residual trapping of CO_2 associated with the flooding process. Relative permeability hysteresis curves provide a convenient way to evaluate these effects. The curves can be measured directly from experiments with sufficient data points or generated from empirical correlations by fitting them to limited data (Juanes et al., 2006; Land, 1968; Larsen and Skauge, 1998).

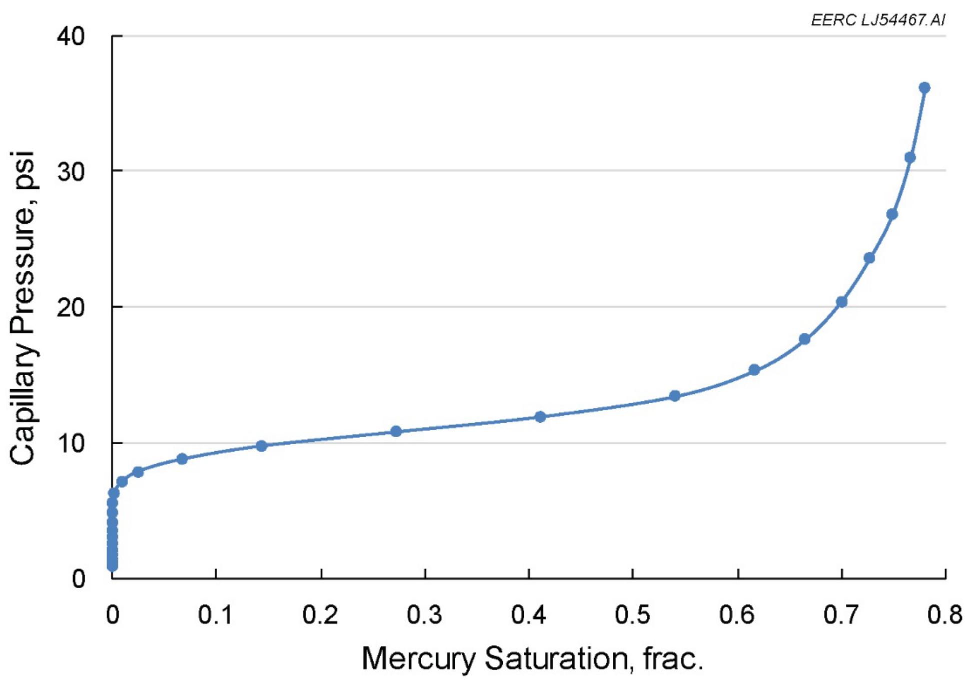

Fig. 5. Capillary pressure curve of a rock sample from the main sandstone in the reservoir.

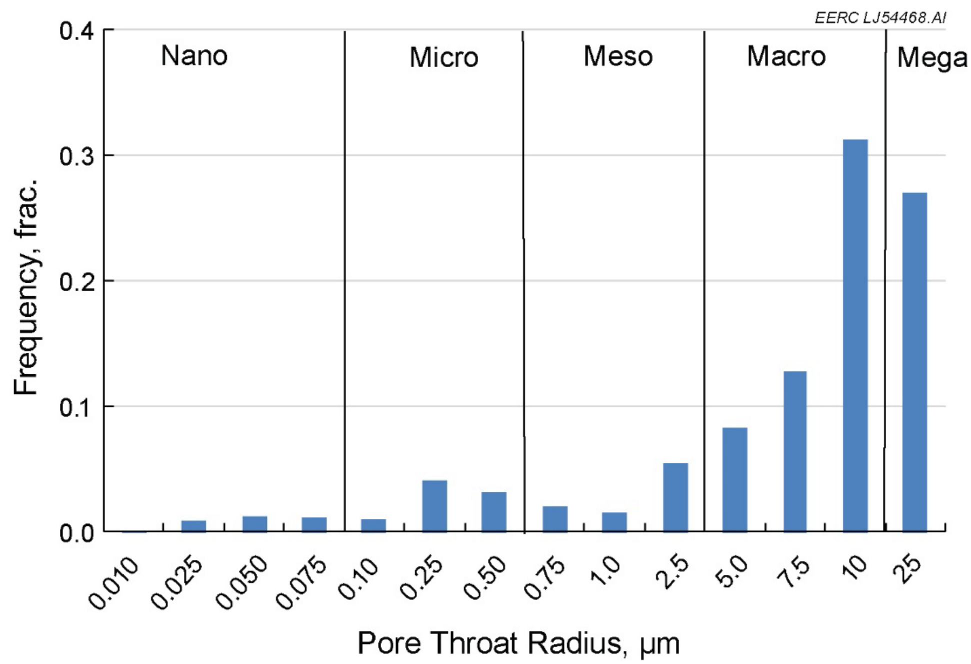

Fig. 6. PSD of a rock sample from the main sandstone in the reservoir.

In this study, relative permeability hysteresis was measured using a clean sandstone core sample, collected from a monitoring well at a depth of 4533 ft. Table 1 contains the measured physical properties of the core sample and the oil used in the procedure. Based upon the reservoir and fluid properties, multicontact miscible flooding occurs in the Bell Creek oil field, therefore, the IFT between CO_2 and oil is minimized during the CO_2 EOR operations. However, the CO_2-oil IFT may decrease gradually in the reservoir since CO_2 injection is conducted progressively across the field. The decreasing IFT is of great interest for miscible/near-miscible CO_2 EOR processes including WAG injection scenarios (Fatemi et al., 2012). Because gas-liquid relative permeabilities change with IFT, especially when IFT becomes low, it is necessary to allow enough contact between CO_2 and oil in the gas-liquid relative permeability hysteresis measurement process. Following the experimental procedure outlined by Fatemi et al. (2012) for low CO_2-oil IFT conditions, CO_2 injection and oil injection were selected for the drainage and imbibition cycles, respectively. Steady-state relative permeability tests were performed using the experimental setup shown in Fig. 7 to derive the relative permeability curves of the gas phase. The experiments were conducted under reservoir conditions (2350 psi and 108°F for confining pressure and temperature, respectively). The pressure profiles for the drainage (CO_2 injection) and imbibition (oil injection) processes are shown in Fig. 8 and Fig. 9, respectively. The plots demonstrate that steady-state displacement was in both drainage and imbibition processes after 1000 seconds.

Table 1
Physical Properties of the Core Used in Relative Permeability Hysteresis Measurements.

Parameter	Value	Unit
Diameter	0.97	in.
Length	1.91	in.
Weight	44.37	g
Grain Density	2.65	g/cm^3
Porosity	0.26	fraction
Permeability	1052	mD
Residual Oil Saturation	0.31	fraction

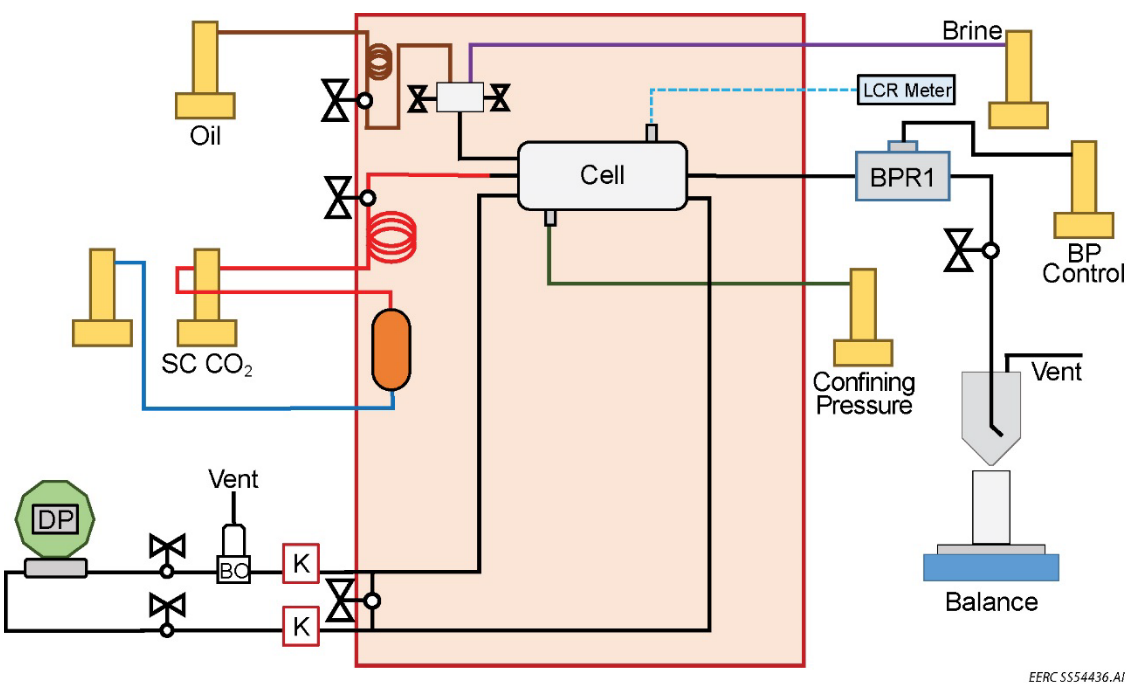

Fig. 7. Experimental setup for relative permeability hysteresis measurement.

The measured relative permeability curves for the gas branch (Fig. 10) clearly show a hysteretic effect between the CO_2 relative permeability curves during drainage and imbibition processes. The irreducible (or trapped) gas saturation increases from 0.07 in the drainage process to 0.19 in the imbibition process, which means a considerable amount of CO_2 was trapped in the core sample during the cycle.

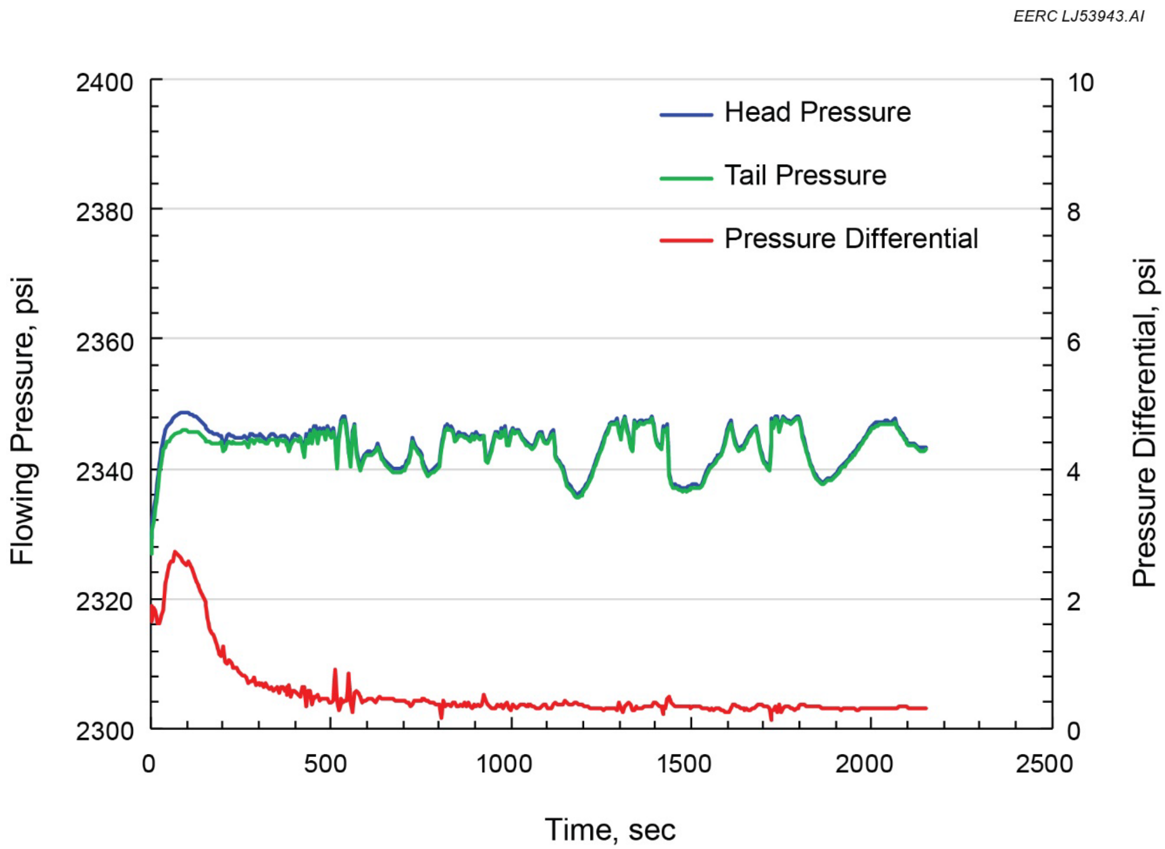

Fig. 8. Pressure profile in the drainage process (CO_2 injection).

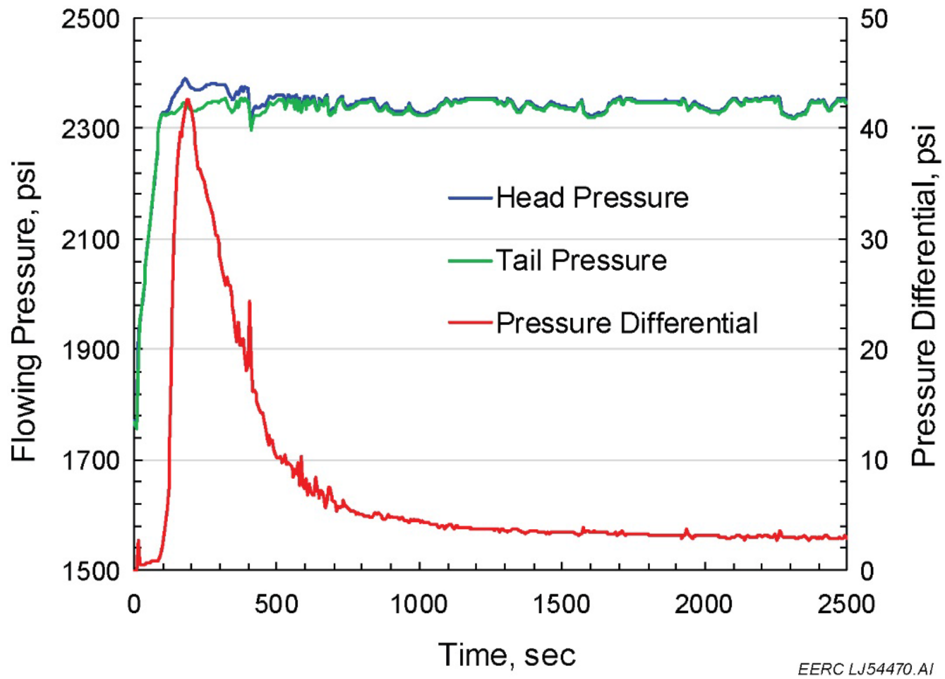

Fig. 9. Pressure profile in the imbibition process (oil injection).

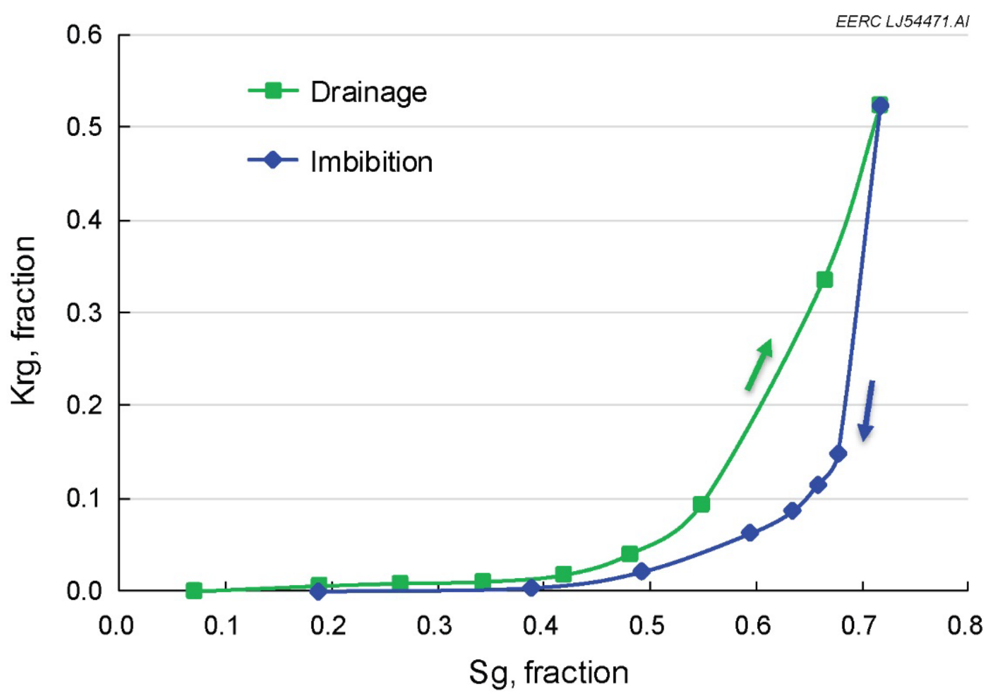

Fig. 10. Relative permeability curves for CO_2 in the drainage and imbibition processes showing a clear hysteretic effect.

4. SOLUBILITY TRAPPING OF CO_2

Aside from residual trapping, solubility trapping of CO_2 is also critical for CO_2 EOR and associated storage. CO_2 dissolution in oil is one of the primary mechanisms for CO_2 EOR, in which dissolved CO_2 changes the oil's physical properties, yielding important benefits to recovery. Through this process, oil volume swells and viscosity reduces, which effectively increase the oil mobility and, thus, oil recovery (Emera and Sarma, 2007). However, the results of this process differ with changing pressure, oil composition, and impurities in the CO_2 stream (Srivastava et al., 1999). Another complication is posed by changing fluid saturations within the reservoir (decreasing oil saturation relative to water saturation). Within the oil phase specifically, the CO_2 EOR process preferentially mobilizes "lighter" hydrocarbon species (short-chain hydrocarbons) in comparison to "heavier" hydrocarbon species (long-chain hydrocarbons) (Hawthorne et al., 2014), resulting in changing oil composition over time. Therefore, fluid characterization and CO_2 solubility need to be studied carefully for a reasonable prediction of associated CO_2 storage which occurs during CO_2-based EOR.

Detailed fluid characterization work has been conducted for the PCOR Partnership study oil using various PVT (pressure–volume–temperature) experiments at reservoir temperature (108°F), including saturation pressure, separator, constant composition expansion, differential liberation, and swelling tests. These tests accurately measured the oil/gas composition, saturation pressure, fluid density, viscosity, formation volume factor, and oil swelling with CO_2, etc. Based on the experimental results, the physical properties of the reservoir fluids can be precisely characterized (Hawthorne et al., 2016). The original and residual oil compositions are shown in Table 2, where considerable medium hydrocarbons are left in the residual oil after pressure depletion. The interactions between CO_2 and these hydrocarbons are important for CO_2 EOR and associated storage performance.

Table 2
Composition of the Crude Oil in the Bell Creek Oil Field.

Oil Composition	**Mole Fraction**	
Component	Original	Residual
CO_2	0.0042	0
N_2	0.0019	0
CH_4	0.1909	0
C_2H_6	0.0033	0.0009
C_3H to NC_4	0.0428	0.0370
IC_5 to C07	0.1526	0.1881
C08 to C13	0.2860	0.3606
C14 to C24	0.1997	0.2523
C25 to C36+	0.1184	0.1612

A series of swelling tests were performed by Core Laboratories Inc. to determine the interactions between CO_2 and oil, especially for CO_2 solubility and the oil-swelling factor, which is defined as the volume of fluid at current saturation pressure divided by the volume of reservoir oil at initial saturation pressure. CO_2 solubility in oil is affected by reservoir temperature, oil saturation pressure, and density, etc. The solubility generally decreases with temperature but increases with oil saturation pressure and density (Perera et al., 2016). Table 3 clearly illustrates the relationship between CO_2 solubility and key parameters of oil under reservoir conditions. The reservoir oil has a strong ability to dissolve CO_2: 0.48 mole fraction of CO_2 can be dissolved in the oil when the oil saturation pressure increases to 1505 psi. Meanwhile, oil viscosity decreases from 2.22 to 0.86 and oil volume swells to 23%, respectively.

Both analytical and numerical correlations have been developed to predict the interactions between oil and CO_2 (Emera and Sarma, 2007; Mulliken and Sandler, 1980). Analytical correlations can be used to calculate the parameters quickly when the system is simple, while numerical correlations are usually used with simulation models to compute the thermodynamic properties of fluids in complex systems.

Table 3
Interactions Between CO_2 and Reservoir Oil at 108°F.

CO_2	**Oil**			
Solubility, mol. frac.	Saturation Pressure, psi	Density, lb/ft^3	Viscosity, cP	Swelling Factor, vol/vol
0.00	925	49.23	2.221	1.0000
0.18	1038	48.64	1.766	1.0668
0.33	1231	49.19	1.316	1.1377
0.48	1505	50.20	0.859	1.2301

To couple with the complicated geologic conditions and strong heterogeneity in the reservoir, a numerical correlation (PVT model with cubic equation of state [EOS]) was developed to investigate the CO_2–oil–water interactions in this study. The PVT model has seven components: CO_2 as a single component and other six components lumped together (N_2–C2, C3–C4, C5–C7, C8–C13, C14–C24, and C25–C36). The Peng–Robinson (PR) EOS was applied to fine tune the model using Computer Modelling Group's (CMG's) WINPROP® module. Experimental data from saturation pressure, separator, constant composition expansion, differential liberation, and swelling tests were matched at reservoir temperature (108°F) to make sure the model can accurately predict the phase behavior of the reservoir fluids. Fig. 11 shows that the PVT model can capture the CO_2 solubility and oil-swelling behavior satisfactorily.

5. CASE STUDY

Reservoir simulation provides a useful means to predict fluid flow behavior in reservoirs with strong heterogeneity and complicated phase behavior. A large-scale simulation model with a total of 859,362 cells (259 × 158 × 21) and 102 wells was constructed to simulate the reservoir performance with CO_2 EOR operations. Satisfactory history-matching results through the primary production, waterflooding, and CO_2-flooding stages showed that the model is able to capture the flow dynamics in the reservoir. Details of the modeling and simulation work have been reported by Jin et al. (2017b). Since relative permeability hysteresis requires greater simulation time and sensitivity analysis of hysteretic effect requires a model with a fast running speed, a smaller five-spot simulation model, as shown in Fig. 12, was clipped from the comprehensive reservoir-scale model to investigate the effects of relative permeability hysteresis and solubility on associated CO_2 storage performance. The five-spot model has five wells for fluid injection/production and also keeps the original reservoir heterogeneity in the model. Its fast running speed makes it possible to conduct sensitivity analysis on residual and solubility trapping effects efficiently.

Several relative permeability hysteresis models, including Land's trapping model, Carlson's hysteresis model, and Killough's hysteresis model, are available to predict the effects of hysteresis on oil recovery and associated storage (Fatemi et al., 2012; Land, 1968; Larsen and Skauge, 1998). In this study, Land's model was used in simulation cases to evaluate the effect of hysteresis on CO_2 flood performance. Based on the measured CO_2 relative permeability hysteresis curves shown in Fig. 10, three different residual CO_2 saturations (0.1, 0.2, and 0.3) were considered in the study

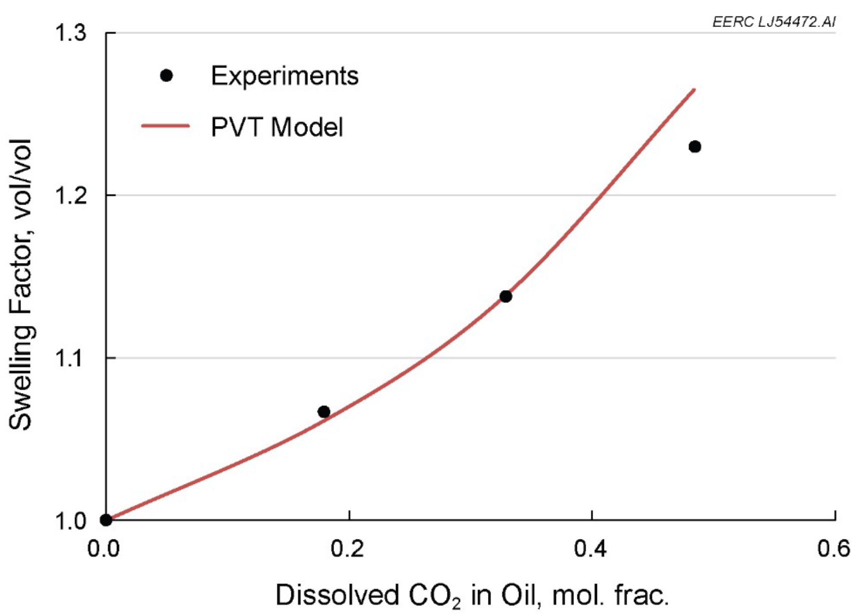

Fig. 11. Correlation between CO_2 solubility and oil-swelling factor.

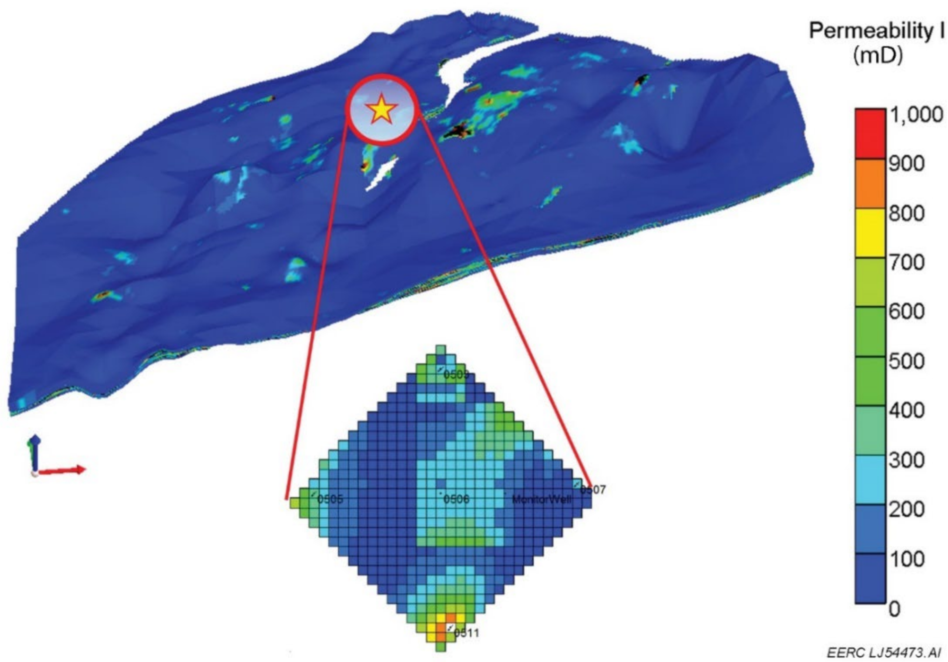

Fig. 12. Simulation model with different scales for the Bell Creek oil field.

to span a range of possible CO_2-trapping scenarios. Fig. 13 shows the comparison of incremental oil recovery for the five-spot model CO_2 EOR simulation cases with and without relative permeability hysteresis. The results indicate relative permeability hysteresis does not have a significant impact on oil recovery in this model. Oil recovery factor is slightly higher when the residual CO_2 saturation is 0.3, but the difference is negligible between other cases. However, the effect of relative permeability hysteresis on total associated CO_2 storage is obvious, as shown in Fig. 14. More CO_2 is stored in the reservoir when residual CO_2 saturation is high, as is expected. Quantitatively, a difference of approximately 20% of total trapped CO_2 was noted between a case without hysteresis (referred as base case hereinafter) applied and a case with hysteresis applied and an assumed residual CO_2 saturation of 0.3 as indicated in Fig. 15. Fig. 16 clearly shows that the residually trapped CO_2 has increased over 220% for the case of 0.3 residual gas saturation compared to the base case.

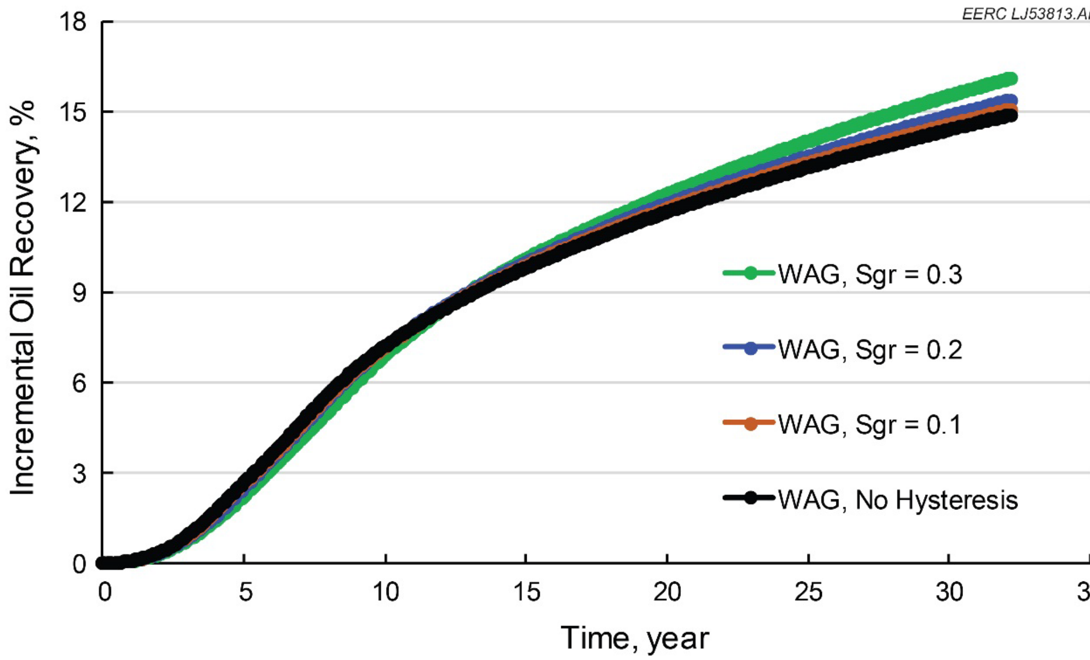

Fig. 13. Comparison of incremental oil recovery for cases with different residual CO_2 saturations.

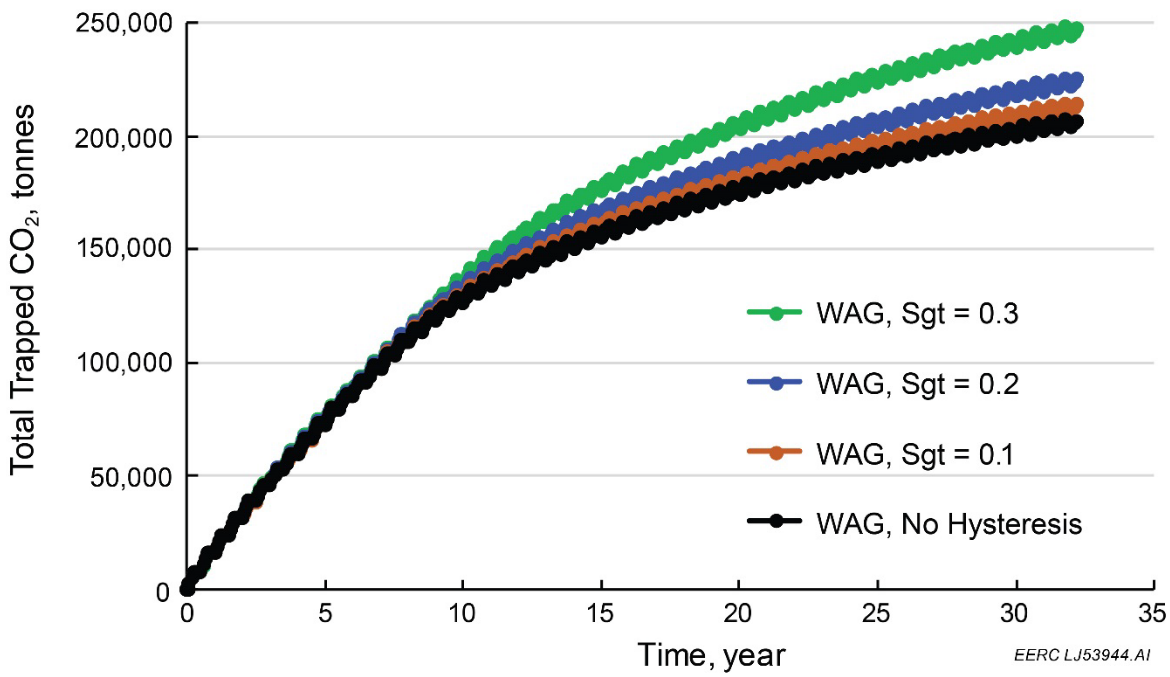

Fig. 14. Comparison of total CO_2 trapped for cases with different residual CO_2 saturations.

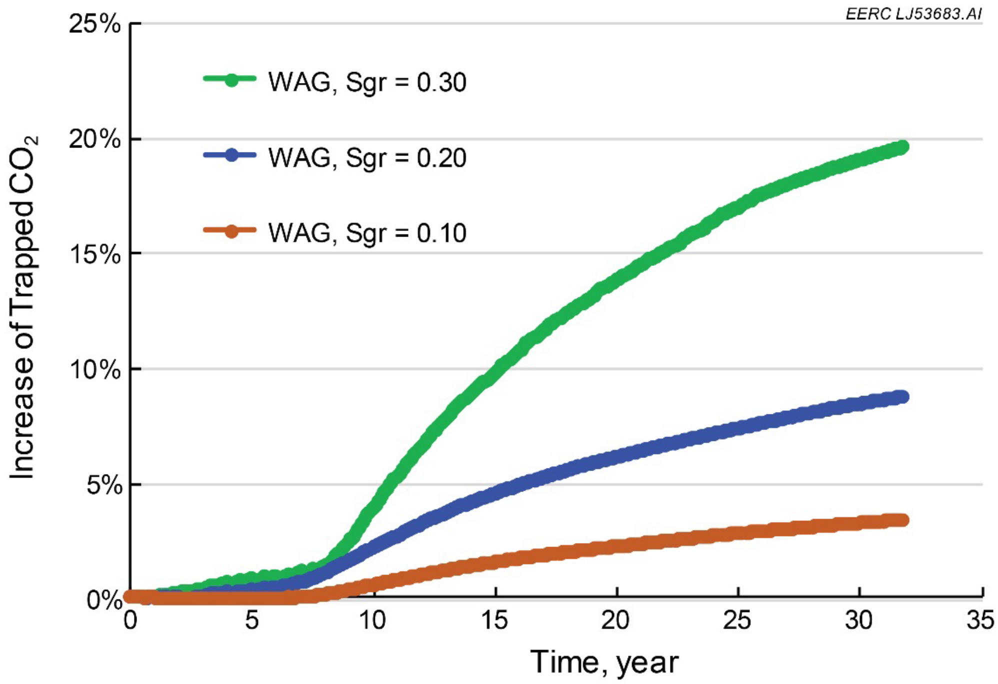

Fig. 15. Increase of total trapped CO_2 compared to the case without hysteresis effect.

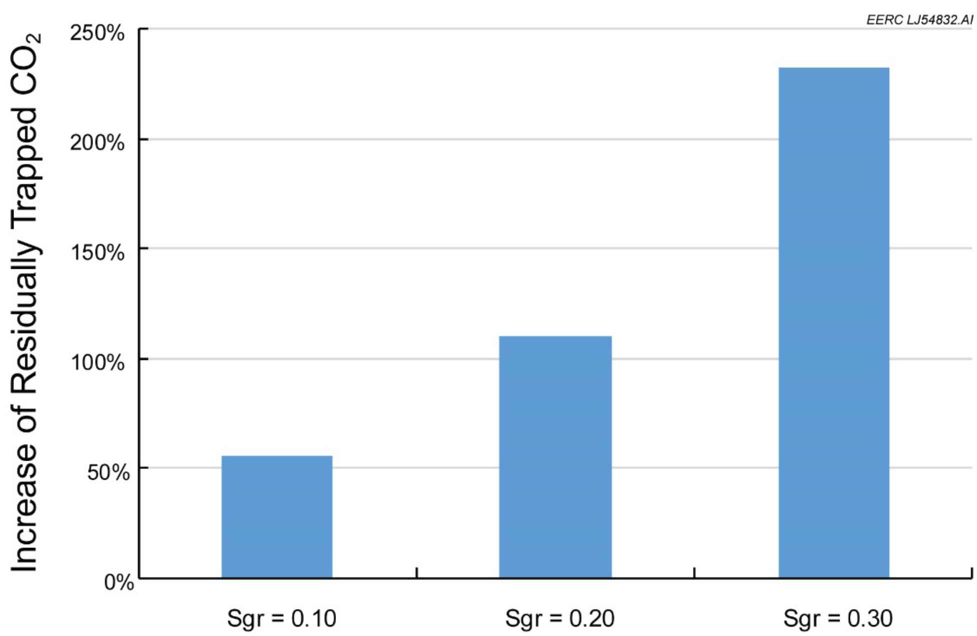

Fig. 16. Increase of residually trapped CO_2 compared to the case without hysteresis effect.

Simulations accounting for CO_2 dissolution in water and oil were conducted together with the hysteresis cases since the solubility correlation has been included in the simulation model. The results of cases assuming different residual CO_2 saturations are shown in Fig. 17. The results indicate CO_2 solubility in oil is much greater (≥5 times) than that of water in the pore volume. A part of residual oil after waterflooding (Sorw) is moved by CO_2 and becomes movable oil (Som = Sorw – Sorm) in the reservoir. This movable oil is then produced to the surface via oil producers, and the CO_2 in the produced oil is separated and continually recycled, i.e., reinjected into the reservoir. However, not all of the movable oil is produced to the surface because of the limitation of producing time (32 years in this study). CO_2 continues to interact with the remaining residual oil (Sorm), dissolving into it and being trapped there after EOR operations cease. As such, the higher the Sorm, the greater the CO_2 trapping potential in residual oil. Residual oil saturation after waterflooding is usually 0.3 or greater in most conventional oil reservoirs, and a considerable quantity of residual oil still remains in the pore space after CO_2 EOR operations. Thus these oil reservoirs could be great candidates for CO_2 storage. The simulation results also show that more CO_2 is dissolved when the trapped CO_2 saturation is higher, as more CO_2 is available to interact with oil and water in the pore space. The dissolved CO_2 in water under different residual gas saturations is also different, but the difference is too small to distinguish in Fig. 17 as the quantities of dissolved CO_2 are 20045, 20278, 20829, and 21871 tonnes for the cases displayed from left to right in the figure, respectively.

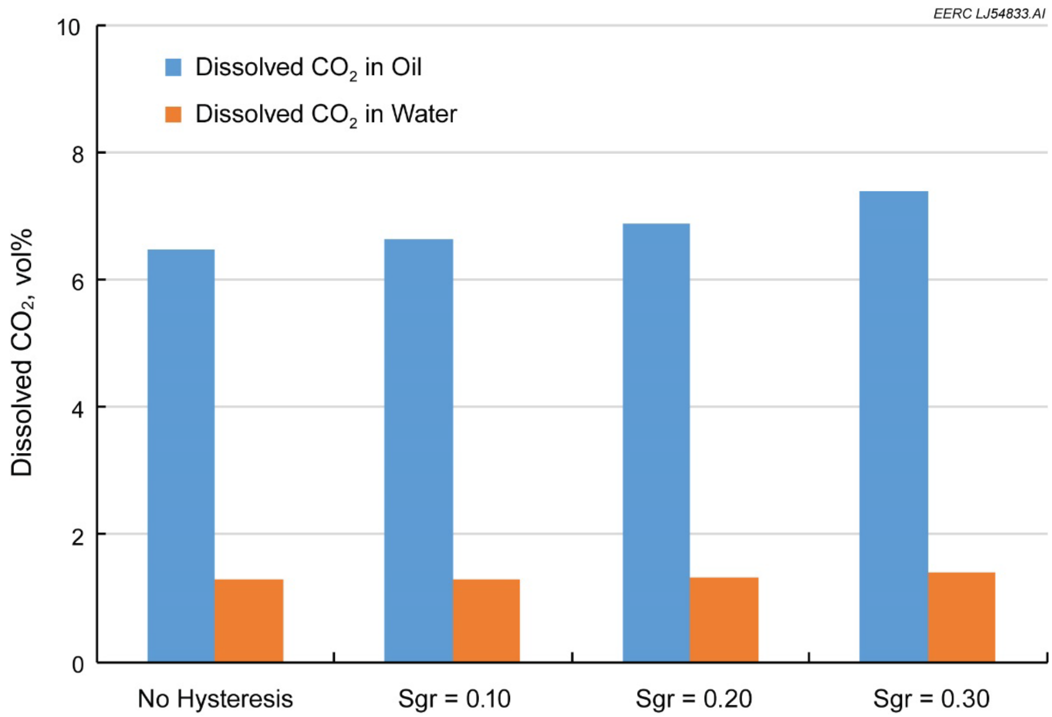

Fig. 17. Comparison of simulated dissolved CO_2 for cases with different residual CO_2 saturations.

6. CONCLUSION

Large-scale CO_2-flooding operations are in progress in the Bell Creek oil field. Encouraging oil production performance shows the success of the EOR project. Simultaneously, a considerable quantity of associated CO_2 storage has occurred in the reservoir. In this study, CO_2-trapping mechanisms in the reservoir associated with EOR operations were analyzed. Two of the primary CO_2-trapping mechanisms responsible for associated CO_2 storage in the Bell Creek oil field, residual trapping and solubility trapping, were discussed in detail. The main findings include the following:

1. Production and injection data were analyzed in the CO_2-flooding stage. Despite the continued improvement of oil production during flooding, the rate of associated CO_2 storage decreased after 2 years. The results indicate the flow network/channels for CO_2 has been well established between injectors and producers in the reservoir.

2. Over 50 core plugs were collected from the reservoir to characterize rock properties. Mineralogical analysis and capillary pressure measurements showed that the mineral composition and PSD in the reservoir are favorable for both CO_2 EOR and associated storage.
3. The reservoir oil was characterized based on PVT experiments and PR EOS modeling. Results showed that the reservoir oil has a strong ability to dissolve CO_2, which not only improves the mobility of residual oil in the reservoir, but also traps a considerable quantity of CO_2 in the reservoir – over 100 thousand tonnes in a five-spot pattern reservoir section under study.
4. Steady-state relative permeability tests were performed to derive gas-phase relative permeability curves using a clean sandstone core sample collected from a monitoring well in the reservoir. The irreducible (or trapped) gas saturation increases from 0.07 in the drainage process to 0.19 in the imbibition process due to the relative permeability hysteresis effects.
5. The relative permeability hysteresis curves were integrated within a five-spot simulation model to investigate the effect of residual trapping on CO_2 EOR and storage performance. Results showed that oil recovery factor and associated CO_2 storage could increase 1.21% and 20%, respectively, considering relative permeability hysteresis with a residual CO_2 saturation of 0.3.
6. The five-spot simulation model was also used to investigate solubility trapping of CO_2 in the reservoir. Based on the fluid properties and reservoir conditions in the Bell Creek oil field, CO_2 solubility in oil is much greater (≥5 times) than that in water.

ACKNOWLEDGMENTS

This work was performed under U.S. Department of Energy National Energy Technology Laboratory Cooperative Agreement No. DE-FC26-05NT42592. The EERC would like to thank Denbury Resources Inc. (Denbury) for providing necessary data to perform this work. Special thanks go to the members of Denbury's Bell Creek team for their valuable input and fruitful discussions. We also thank Computer Modelling Group Ltd. (CMG) for providing us with the simulation software package, which makes the high-performance computation/simulation possible.

DOE DISCLAIMER

This paper was prepared as an account of work sponsored by an agency of the United States Government. Neither the United States Government, nor any agency thereof, nor any of their employees, makes any warranty, express or implied, or assumes any legal liability or responsibility for the accuracy, completeness, or usefulness of any information, apparatus, product, or process disclosed, or represents that its use would not infringe privately owned rights. Reference herein to any specific commercial product, process, or service by trade name, trademark, manufacturer, or otherwise does not necessarily constitute or imply its endorsement, recommendation, or favoring by the United States Government or any agency thereof. The views and opinions of authors expressed herein do not necessarily state or reflect those of the United States Government or any agency thereof.

CONVERSIONS

C:	compressibility, psi^{-1}	× 0.145 kPa^{-1}
d:	diameter, *in*	× 0.0254 m
k:	permeability, *mD*	× 10^{-12} m^2
l:	length, *in*	× 0.0254 m
m:	weight, *g*	× 10^{-3} kg
p_b:	saturation pressure, *psi*	× 6.895 kPa

p_c:	capillary pressure, *psi*	× 6.895 *kPa*
p_e:	reservoir pressure, *psi*	× 6.895 *kPa*
q:	liquid production rate, *bpd*	× $6.625*10^{-3}$ m^3/hr
Q:	cumulative liquid production, *bbl*	× 0.159 m^3
r:	pore throat radius, *µm*	× 10^{-6} *m*
Som	movable oil saturation	× 1 *fraction*
Sorm	residual oil saturation after CO_2 flooding	× 1 *fraction*
Sorw	residual oil saturation after water flooding	× 1 *fraction*
T:	temperature, °*F*	= ([°F] + 459.67) × ⁵⁄₉ *K*
FVF:	formation volume factor, *rb/stb*	× 1 rm^3/sm^3
GOR:	gas-oil ratio, *scf/stb*	× 0.178 m^3/m^3
ρ:	density, lb/ft^3	× 16.02 kg/m^3
σ:	interfacial tension, *dyne/cm*	× 1 *dyne/cm*
Θ:	contact angle between two phases, *degree*	× 1 *degree*
ϕ:	porosity, *fraction*	× 1 *fraction*
µ:	viscosity, *cP*	× 10^{-3} *Pa·s*

REFERENCES

Afonja, G., Hughes, R.G., Nagineni, V., Jin, L., 2012. Simulation study for optimizing injected surfactant volume in a miscible carbon dioxide flood. Proceedings of SPETT Energy Conference and Exhibition, SPE 158220, Port-of-Spain, Trinidad, June 11–13.

Ahmed, T., 2006. Reservoir engineering handbook, Gulf Professional Publishing.

Al-Khdheeawi, E.A., Vialle, S., Barifcani, A., Sarmadivaleh, M., Iglauer, S., 2018. Effect of wettability heterogeneity and reservoir temperature on CO_2 storage efficiency in deep saline aquifers. IJGGC, 68, 216–229.

Al-Menhali, A.S., Krevor, S., 2016. Capillary trapping of CO_2 in oil reservoirs—observations in a mixed-wet carbonate rock. Environ. Sci. Technol., 50 (5), 2727–2734.

Ampomah, W., Balch, R., Cather, M., Rose-Coss, D., Dai, Z., Heath, J., Dewers, T., Mozley, P., 2016. Evaluation of CO_2 storage mechanisms in CO_2 enhanced oil recovery sites—application to Morrow sandstone reservoir. Energy Fuels, 30 (10), 8545–8555.

Bachu, S., Adams, J.J., 2003. Sequestration of CO_2 in geological media in response to climate change—capacity of deep saline aquifers to sequester CO_2 in solution. Energy Conversion and Management, 44 (20), 3151–3175.

Bachu, S., Bennion, B., 2007. Effects of in situ conditions on relative permeability characteristics of CO_2—brine systems. Environ. Geol., 54 (8).

Belhaj, H., Abukhalifeh, H., Javid, K., 2013. Miscible oil recovery utilizing N_2 and/or HC gases in CO_2 injection. J. Petrol. Sci. Eng., 111, 144–52.

Braunberger, J., Hamling, J., Gorecki, C., Miller, H., Rawson, J., Walsh, F., Pasternack, E., Rowe, W., Butsch, R., Steadman, E., Harju, J., 2014. Characterization and time-lapse monitoring utilizing pulsed-neutron well logging. associated CO_2 storage at a commercial CO_2 EOR project. Energy Proc., 63, 3935–3944.

Burnside, N.M., Taylor, M., 2014. .Review and implications of relative permeability of CO_2/brine systems and residual trapping of CO_2. IJGGC, 23, (1–1).

Busch, A., Alles, S., Gensterblum, Y., Prinz, D., Dewhurst, D.N., Raven, M.D., Stanjek, H., Krooss, B.M., 2008. Carbon dioxide storage potential of shales. IJGGC, 2 (3), 297–308.

Emera, M.K., Sarma, H.K., 2007. Prediction of CO_2 solubility in oil and the effects on the oil physical properties. Energy Sources, Part A., 29 (13), 1233–1242.

Ennis-King, J., Paterson, L.I., 2001. Reservoir engineering issues in the geological disposal of carbon dioxide. Proceedings of the 5th International Conference on Greenhouse Gas Control Technologies. Cairns, 1, 290–295.

Fatemi, S.M., Sohrabi, M., Jamiolahmady, M., Ireland, S., 2012. Experimental and theoretical investigation of gas/oil relative permeability hysteresis under low oil/gas interfacial tension and mixed-wet conditions. Energy Fuels, 26 (7), 4366–4382.

Gale, J., Freund, P., 2001. Coal-bed methane enhancement with CO_2 sequestration worldwide potential. Environ. Geosci., 8 (3), 210–217.

Gao, C., Li, X., Guo, L., Zhao, F., 2013, Heavy oil production by carbon dioxide injection. Greenhouse Gases. Sci. Technol., 3 (3), 185–195.

Gorecki, C.D., Harju, J.A., Steadman, E.N., Heebink, L.V., Romuld, L., Hamling, J.A., Sorensen, J.A., Daly, D.J., Jensen, M.D., Peck, W.D., Klapperich, R.J., Votava, T.F., Pekot, L.J,. Ayash, S.C., Ensrud, J.R., 2013. Annual assessment report. Plains CO_2 reduction (PCOR) partnership Phase III Task 12 Deliverable D57 (October 1, 2014 – September 30, 2015) for U.S. Department of Energy National Energy Technology Laboratory Cooperative Agreement No. DE-FC26-05NT42592. Energy & Environmental Research Center: Grand Forks, North Dakota.

Gozalpour, F., Ren, S.R., Tohidi, B., 2005. CO_2 EOR and storage in oil reservoir. Oil & Gas Sci. Technol., 60 (3), 537–46.

Hamling, J.A., Glazewski, K.A., Leroux, K.M., Kalenze, N.S., Bosshart, N.W., Burnison, S.A., Klapperich, R.J., Stepan, D.J., Gorecki, C.D., Richards, T.L., 2016. Monitoring 3.2 million tonnes of CO_2 at the Bell Creek oil field. Energy Proc., 114, 5553–5561.

Hamling, J.A., Gorecki, C.D., Klapperich, R.J., Saini, D., Steadman, E.N., 2013. Overview of the Bell Creek combined CO_2 storage and CO_2 enhanced oil recovery project. Energy Proc., 31 (37), 6402–6411.

Hawthorne, S.B., Miller, D.J., Gorecki, C.D., Sorensen, J.A., Hamling, J.A., Roen, T.D., Harju, J.A., Melzer, S., 2014. A rapid method for determining CO_2/Oil MMP and visual observations of CO_2/oil interactions at reservoir conditions. Energy Proc., 63, 7724–7731.

Hawthorne, S.B., Miller, D.J., Jin, L, Gorecki, C.D., 2016, Rapid and simple capillary-rise/vanishing interfacial tension method to determine crude oil minimum miscibility pressure. pure and mixed CO_2, methane, and ethane. Energy Fuels, 30 (8), 6365–6372.

Holm, L.W., Josendal, V.A., 1974. Mechanisms of oil displacement by carbon dioxide. Journal of Petroleum Technology, 26 (12), 1427–1438.

Holubnyak, Y., Watney, W., Hollenbach, J., Rush, J., Fazelalavi, M., Bidgoli, T., Wreath, D., 2018. Pilot scale CO_2 EOR at Wellington filed in South Central Kansas. SPE-190308, Proceedings of SPE Improved Oil Recovery Conference, Tulsa, OK, April 13.

Iglauer, S., 2011. Dissolution trapping of carbon dioxide in reservoir formation brine–a carbon storage mechanism. InMass Transfer-Advanced Aspects. InTech.

Jia, B., Tsau, J.S., Barati, R., 2017, Role of molecular diffusion in heterogeneous sale reservoirs during CO_2 huff-n-puff. SPE Europec featured at 79th EAGE Conference and Exhibition, Society of Petroleum Engineers.

Jia, W., McPherson, B.J., Pan, F., Xiao, T., Bromhal, G., 2016. Probabilistic analysis of CO_2 storage mechanisms in a CO_2 EOR field using polynomial chaos expansion. IJGGC. 51, 218–229.

Jin, L., Hawthorne, S.B., Sorensen, J.A., Pekot, L.J., Kurz, B.A., Smith, S.A., Heebink, L.V., Herdegen, V., Bosshart, N.W., Torres Rivero, J.A., Dalkhaa, C., 2017a. Advancing CO_2 enhanced oil recovery and storage in unconventional oil play—experimental studies on Bakken shales. Applied Energy, 208, 171–183.

Jin, L., Pekot, L.J., Hawthorne, S.B., Gobran, B., Greeves, A., Bosshart, N.W., Jiang, T., Hamling, J.A. Gorecki, C.D., 2017b. Impact of CO_2 impurity on MMP and oil recovery performance of the Bell Creek Oil Field. Energy Proc., 114, 6997–7008.

Jin, L., Sorensen, J.A., Hawthorne, S.B., Smith, S., Pekot, L.J., Bosshart, N.W., Burton-Kelly, M.E., Miller, D.J., Grabanski, C.B., Gorecki, C.D., Steadman, E.N., 2016, Improving oil recovery by use of carbon dioxide in the Bakken unconventional system—a laboratory investigation. SPE Reservoir Eval. Eng., 20 (3).

Juanes, R., Spiteri, E.J., Orr, F.M., Blunt, M.J., 2006. Impact of relative permeability hysteresis on geological CO_2 storage. Water Resources Research, 42 (12).

Khosrokhavar, R., Griffiths, S., Wolf, K.H., 2014. Shale gas formations and their potential for carbon storage. opportunities and outlook. Environ. Processes, 1 (4), 595–611.

Kovscek, A.R., 2002. Screening criteria for CO_2 storage in oil reservoirs. Petrol. Sci. Technol., 20 (7–8), 841–866.

Krevor, S., Blunt, M.J., Benson, S.M., Pentland, C.H., Reynolds, C., Al-Menhali, A., Niu, B., 2015. Capillary trapping for geologic carbon dioxide storage—from pore scale physics to field scale implications. IJGGC, 40, 221–2237.

Krevor, S., Pini, R., Zuo, L., Benson, S.M., 2012. Relative permeability and trapping of CO_2 and water in sandstone rocks at reservoir conditions. Water Resources Res., 48 (2).

Land, C.S., 1968. Calculation of imbibition relative permeability for two-and three-phase flow from rock properties. SPE Journal, 8 (02), 149–56.

Larsen, J.A., Skauge, A., 1998. Methodology for numerical simulation with cycle-dependent relative permeabilities. SPE Journal, 3 (2), 163–173.

Li, D., Jiang, X., 2014. A numerical study of the impurity effects of nitrogen and sulfur dioxide on the solubility trapping of carbon dioxide geological storage. Appl. Energy, 128, 60–74.

Li, Z., Dong, M., Li, S., Huang, S., 2006. CO_2 sequestration in depleted oil and gas reservoirs—caprock characterization and storage capacity. Energy Conversion and Management, 47 (11), 1372–1382.

Malik, Q.M., Islam, M,R., 2001. CO_2 Injection in the Weyburn field of Canada. optimization of enhanced oil recovery and greenhouse gas storage with horizontal wells. SPE/DOE Improved Oil Recovery Symposium, Society of Petroleum Engineers.

McGrail, B.P., Schaef, H.T., Ho, A.M., Chien, Y.J., Dooley, J.J., Davidson, C.L., 2006. Potential for carbon dioxide sequestration in flood basalts. J. Geophys. Res. Solid Earth, 111, B12.

McGrail, B.P., Schaef, H.T., Spane, F.A., Cliff, J.B., Qafoku, O., Horner, J.A., Thompson, C.J., Owen, A.T., Sullivan, C.E., 2016. Field validation of supercritical CO_2 reactivity with basalts. Environ. Sci. Technol. Letters, 4 (1), 6–10.

Metz, B., Davidson, O., De Coninck, H., Loos, M., Meyer, L., 2005. IPCC special report on carbon dioxide capture and storage. Intergovernmental Panel on Climate Change, Geneva (Switzerland), Working Group III, July 1.

Montana Board of Oil and Gas Conservation. 2017, MBOGC online oil and gas information system. www.bogc.dnrc.mt.gov/WebApps/DataMiner (accessed October 5, 2017).

Mulliken, C.A., Sandler, S.I., 1980. The prediction of CO_2 solubility and swelling factors for enhanced oil recovery. Industr. Eng. Chem. Process Design Devel., 4, 709–711.

Niu, B., Al-Menhali, A., Krevor, S.C., 2015. The impact of reservoir conditions on the residual trapping of carbon dioxide in Berea sandstone. Water Resources Res., 51 (4), 2009–2029.

Perera, M.S., Gamage, R.P., Rathnaweera, T.D., Ranathunga, A.S., Koay, A., Choi, X.A., 2016. Review of CO_2-enhanced oil recovery with a simulated sensitivity analysis. Energies, 9 (7), 481.

Raza, A., Rezaee, R., Bing, C.H., Gholami, R., Hamid, M.A., Nagarajan, R., 2016. Carbon dioxide storage in subsurface geologic medium—a review on capillary trapping mechanism. Egyptian J. Petrol., 25 (3), 367–373.

Raza, A., Rezaee, R., Gholami, R., Rasouli, V., Bing, C.H., Nagarajan, R., Hamid, M.A., 2015. Injectivity and quantification of capillary trapping for CO_2 storage—a review of influencing parameters. J. Natural Gas Sci. Eng., 26 (510), 7.

Ross, D.J., Bustin, R.M., 2009. The importance of shale composition and pore structure upon gas storage potential of shale gas reservoirs. Marine Petrol. Geol., 26 (6), 916–927.

Ruprecht, C., Pini, R., Falta, R., Benson, S., Murdoch, L, 2014. Hysteretic trapping and relative permeability of CO_2 in sandstone at reservoir conditions. IJGGC, 27, 15–27.

Shelton, J.L., McIntosh, J.C., Hunt, A.G., Beebe, T.L., Parker, A.D., Warwick, P.D., Drake, R.M., McCray, J.E., 2016. Determining CO_2 storage potential during miscible CO_2 enhanced oil recovery—noble gas and stable isotope tracers. IJGGC, 51, 239–253.

Soltanian, M.R., Amooie, M.A., Gershenzon, N., Dai, Z., Ritzi, R., Xiong, F., Cole, D.R., and Moortgat, J., 2017. Dissolution trapping of carbon dioxide in heterogeneous aquifers. Environ. Sci. Technol., 51 (13), 7732–7741.

Spiteri, E.J., Juanes, R., Blunt, M.J., Orr, F.M., 2008. A new model of trapping and relative permeability hysteresis for all wettability characteristics. SPE Journal, 13 (03), 277–288.

Srivastava, R.K., Huang, S.S., Dong, M., 1999. Asphaltene deposition during CO_2 flooding. SPE Product. Facil., 14 (04), 235–245.

Szulczewski, M.L., Hesse, M.A., Juanes, R., 2013. Carbon dioxide dissolution in structural and stratigraphic traps. J. Fluid Mechanics, 736, 287–315.

Verma, M.K., 2015. Fundamentals of carbon dioxide-enhanced oil recovery (CO_2-EOR). A supporting document of the assessment methodology for hydrocarbon recovery using CO_2-EOR associated with carbon sequestration. U.S. Department of the Interior, U.S. Geological Survey.

Wong, S., Law, D., Deng, X., Robinson, J., Kadatz, B., Gunter, W.D., Jianping, Y., Sanli, F., Zhiqiang, F., 2007. Enhanced coalbed methane and CO_2 storage in anthracitic coals—Micro-pilot test at South Qinshui, Shanxi, China. IJGGC, 1 (2), 215–222.

Zhang, Y., Huang, S.S., Luo, P., 2010. Coupling immiscible CO_2 technology and polymer injection to maximize EOR performance for heavy oils. J. Canadian Petrol. Technol., 49 (05), 25–33.

Zuo, L., Benson, S.M., 2014. Process-dependent residual trapping of CO_2 in sandstone. Geophys. Res. Letters, 41 (8), 2820–2826.